Two-channel autofluorescence analysis for oral cancer

Tze-Ta Huang
Ken-Chung Chen
Tung-Yiu Wong
Chih-Yang Chen
Wang-Ch Chen
Yi-Chun Chen
Ming-Hsuan Chang
Dong-Yuan Wu
Teng-Yi Huang
Shoko Nioka
Pau-Choo Chung
Jehn-Shyun Huang

Two-channel autofluorescence analysis for oral cancer

Tze-Ta Huang,[a,b] **Ken-Chung Chen,**[a,b] **Tung-Yiu Wong,**[a,b] **Chih-Yang Chen,**[c] **Wang-Ch Chen,**[c] **Yi-Chun Chen,**[b] **Ming-Hsuan Chang,**[d] **Dong-Yuan Wu,**[d] **Teng-Yi Huang,**[d] **Shoko Nioka,**[e] **Pau-Choo Chung,**[f,*] **and Jehn-Shyun Huang**[a,b,*]
aNational Cheng Kung University Hospital, Department of Stomatology, Division of Oral and Maxillofacial Surgery, Tainan, Taiwan
bNational Cheng Kung University Medical College and Hospital, Institute of Oral Medicine, Tainan, Taiwan
cDelta Electronics, Inc., Tainan, Taiwan
dNational Cheng Kung University, Institute of Computer and Communication Engineering, Tainan, Taiwan
eUniversity of Pennsylvania, Department of Radiology, Philadelphia, Pennsylvania, United States
fNational Cheng Kung University, Department of Electrical Engineering, Tainan, Taiwan

Abstract. We created a two-channel autofluorescence test to detect oral cancer. The wavelengths 375 and 460 nm, with filters of 479 and 525 nm, were designed to excite and detect reduced-form nicotinamide adenine dinucleotide (NADH) and flavin adenine dinucleotide (FAD) autofluorescence. Patients with oral cancer or with precancerous lesions, and a control group with healthy oral mucosae, were enrolled. The lesion in the autofluorescent image was the region of interest. The average intensity and heterogeneity of the NADH and FAD were calculated. The redox ratio [(NADH)/(NADH + FAD)] was also computed. A quadratic discriminant analysis (QDA) was used to compute boundaries based on sensitivity and specificity. We analyzed 49 oral cancer lesions, 34 precancerous lesions, and 77 healthy oral mucosae. A boundary (sensitivity: 0.974 and specificity: 0.898) between the oral cancer lesions and healthy oral mucosae was validated. Oral cancer and precancerous lesions were also differentiated from healthy oral mucosae (sensitivity: 0.919 and specificity: 0.755). The two-channel autofluorescence detection device and analyses of the intensity and heterogeneity of NADH, and of FAD, and the redox ratio combined with a QDA classifier can differentiate oral cancer and precancerous lesions from healthy oral mucosae. © *The Authors. Published by SPIE under a Creative Commons Attribution 4.0 Unported License. Distribution or reproduction of this work in whole or in part requires full attribution of the original publication, including its DOI.* [DOI: 10.1117/1.JBO.24.5.051402]

1 Introduction

Oral squamous cell carcinoma (OSCC) is the most common malignant disease of oral mucosa.[1] The average 5-year survival rate is ~60%.[2] The incidence and severity of OSCC are increasing worldwide, especially in Taiwan.[3] The diagnosis of oral cancer has relied heavily on lesion biopsies, which are time-consuming and uncomfortable for patients.[4] In view of these disadvantages, noninvasive oral cancer detection methods, such as a brush biopsy,[5] autofluorescence imaging,[6,7] and toluidine blue staining[8,9] have been used. Nevertheless, the physician's experience is critical when using current methods. Developing the visual detection of chemoluminescence and tissue fluorescence for diagnosing oral cancer might improve detection and allow us to earlier identify potentially malignant lesions.[7]

Different autofluorescence intensities have been reported[10] for animal tumor cells and healthy cells; thus, researchers are now looking for spectral characteristics,[6] using fluorescence spectroscopy[11] observing the autofluorescence imaging of biopsy tissue by large equipment, and using autofluorescence imaging methods in a clinical trial.[12] We previously[7] used a light source with one wavelength to excite the autofluorescence of tissue. The light source was only for direct vision; thus, a camera was needed to document the images. We introduced using the standard deviation of the intensity of an autofluorescence image to determine the heterogeneity of a lesion.[7] Tumor heterogeneity can be characterized as genetic, phenotypic, or functional. Genetic and phenotypic biomarkers provide statistical measurements, and functional measures characterize dynamic tumor behavior. Functional measures include cellular metabolism, oxygen consumption, and blood perfusion. Specifically, cellular metabolism, which is altered in cancer patients, is a prominent marker of tumor heterogeneity.[13] The standard deviation of an autofluorescence image primarily indicates a change inside the heterogeneous lesion. The higher heterogeneity in oral cancer tissue than in healthy oral mucosa might reflect the heterogeneity of cancer.

Autofluorescence is generated by a tissue matrix or fluorophores in living cells.[14] During carcinogenesis, metabolism and the structure of tissue change. The Warburg effect shows that aerobic glycolysis in cells generates lactate,[15] boosts production of reduced-form nicotinamide adenine dinucleotide (NADH), and raises the value of the NADH/NADH + flavin adenine dinucleotide (FAD) ratio (redox ratio).[16] An increase in the redox ratio implies that the cell is hypoxic. The redox ratio has been used to show the metabolic differences between healthy and tumorous tissue and between indolent and aggressive tumors.[17] NADH intensity is higher in cancerous and precancerous tissue than in healthy tissue.[18] The redox ratio is also used to detect melanoma, breast cancer, and pancreatic cancer.[17,19]

*Address all correspondence to: Pau-Choo Chung, E-mail: pcchung@ee.ncku.edu.tw; Jehn-Shyun Huang, E-mail: huangjs@mail.ncku.edu.tw
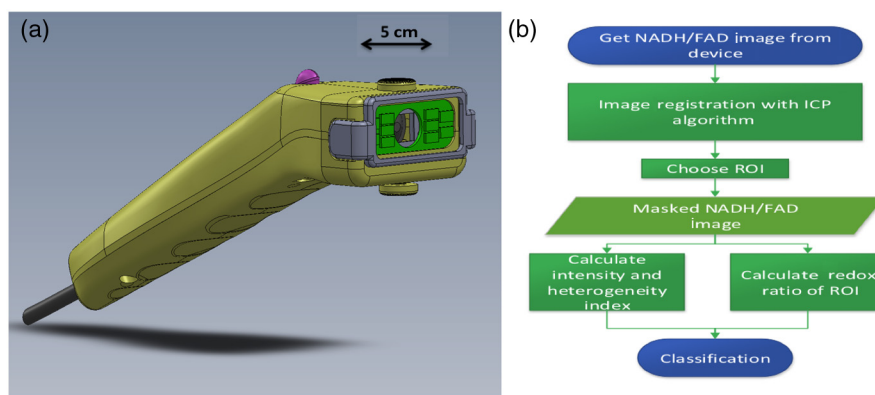
Fig. 1 (a) Two-channel autofluorescence detection device designed for this study. Two LED, two filters, and camera were intergrated with automatic switching. (b) The flowchart of this research.

The intensity and heterogeneity of autofluorescence and the redox ratio might be for detecting cancer. In this present study, we used two-channel light source to detect two fluorescent metabolites, NADH and FAD, and computed their intensity, heterogeneity, and redox ratios to detect oral cancer.

2 Materials and Method

This study, conducted in the Division of Oral and Maxillofacial Surgery, was approved by the Institutional Review Board of National Cheng Kung University Hospital (IRB No: B-ER-104-035). All participants signed written informed consent forms.

2.1 Autofluorescence Imaging Device

2.1.1 Component of the device

We used a light-sensitive (0.01 lux) CCD camera with a 90-deg wide-angle lens and a 5-cm focus in the low-light environment of the oral cavity.

To excite the maximum quantity of NADH and FAD auto-fluorescence, the peak of their absorption spectra was chosen. The wavelengths of 375- and 460-nm LED for NADH and FAD, respectively, are based on their corresponding absorption spectra.[20] In addition, the LED components of our device have a low radiation hazard, which is confirmed by the Société Générale de Surveillance (SGS).[21] The two LED components are continuous wave lamps; each has a narrow spectral wave-length. The 375-nm LED wavelength ranges from 350 to 410 nm, and the radiation hazards comply with the limit level for the Exempt Group. The 460-nm LED wavelength ranges from 410 to 530 nm, and the radiation hazards comply with the limit level for risk group 1. Two emission filters with center wavelengths of 479 and 525 nm were chosen for this study because of their transmission spectra.[20] The parameters and specifications of the device are listed in Appendix A.

2.1.2 Design of the device

To have a redox ratio image, NADH and FAD autofluorescences must be captured in the same location, but no commercial device capable of doing that was available. Therefore, we designed a handheld device with LEDs at 375 and 460 nm as an excitation light source for NADH and FAD, a CCD camera covered with filters at 479 and 525 nm to generate an autofluorescence image,

and a minimotor to switch filters. This device was connected to a computer to instantly view the image [Fig. 1(a)].

The device will turn on 460-nm LEDs and set itself to the 525-nm filter. When ready, the operator can examine autofluor-escence image excited by 460-nm blue light to locate the lesion. Once the lesion is located, pressing a button will capture the two images excited by the 460-nm LEDs and the 375-nm LEDs, respectively. Changing filters using the minimotor and LED lighting takes about 1 s [image acquiring flowchart: Fig. 1(b)].

2.2 Analysis Method

The NADH and FAD autofluorescence images were concurrently captured using the same device [Figs. 2(a) and 3]. However, there were still small differences between the two images because the operator's hand was unsteady when holding the device, or because of the patient's breathing. We, therefore, selected the iterative closest point (ICP) algorithm[22] to correct the difference in location between the two images [Fig. 2(c)] by minimizing the difference between two clouds of points. The ICP algorithm uses the following steps:

2.2.1 Extract point clouds from NADH/FAD autofluorescence images

The point cloud for registration is normally obtained from salient regions in the images. For example in Fig. 2(a), there is a tooth with strong intensities and sharp edges in the middle of the patient's images. Therefore, we make that tooth an important feature for extracting point cloud for registration. The simplest method to obtain point cloud from an autofluorescence image is to segment the region using thresholding [Fig. 2(b)]. However, if there is no tooth in the images, we will use the salient edges, such as the boundary edge around the tongue, or the boundary edge around the lips for the registration. To obtain reliable edges, we use a Canny edge detector. Edges with strong signal were used for registration.

Once the point clouds are obtained for the two images, the five ICP algorithm steps listed below are done. (Inputs: reference point clouds, RP; source point clouds, SP; iterations, K; threshold of the error, ε; Output: refined transformation). (1) Find the closest point in the RP for each point in SP. (2) Calculate the rotation parameter R and translation parameter T using singular value decomposition. (3) Apply the translation of R and T to the RP. (4) Calculate the error ER between RP and
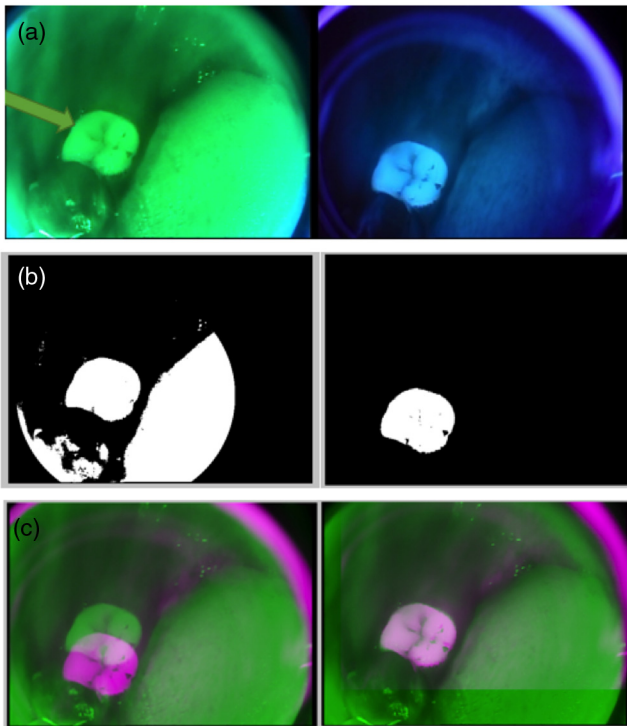
Fig. 2 (a) The 375- and 460-nm wavelengths were excited and detected using 479-nm (right) and 525-nm (left) filters. The arrow points to a tooth. (b) Masked logical image for point-cloud conversion (left is 525 nm, right is 479 nm). (c) Images before (left) and after (right) using the ICP algorithm (purple is 479 nm and green is 525 nm).

SP using root mean square. (5) Repeat steps 1 to 4 if ER > ε and the number of iterations is <K.

2.2.2 Selecting the region of interest

The patients' attending physicians who are also the authors, selected the lesion sites as a region of interest (ROI) to avoid the noise produced by shadows or teeth (Fig. 3). Patient records and the white-light digital photos taken before the data analysis were used as a reference. Each ROI was saved with a binary mask image, and only the region with binary mask was analyzed (Fig. 4).

2.2.3 Autofluorescence intensity and heterogeneity

The autofluorescence images from the excitation wavelengths between 375 and 460 nm and detected using of 479- and 525-nm filters were analyzed for average intensity and the standard deviation, respectively, representing the heterogeneity using the algorithm previously described.[7]

2.2.4 Redox ratio

We used NADH/(NADH + FAD) as the redox ratio to describe the metabolic state of the tissue. The NADH autofluorescence image was excited using a 375-nm LED and filtered using a 479-nm emission filter; the FAD autofluorescence image was excited using a 460-nm LED and filtered using a 525-nm filter. We used $I_n(x,y)$ as the NADH autofluorescence image, and $I_f(x,y)$ as the FAD autofluorescence image. A pixel-wise redox ratio $I_r(x,y)$ image is defined as
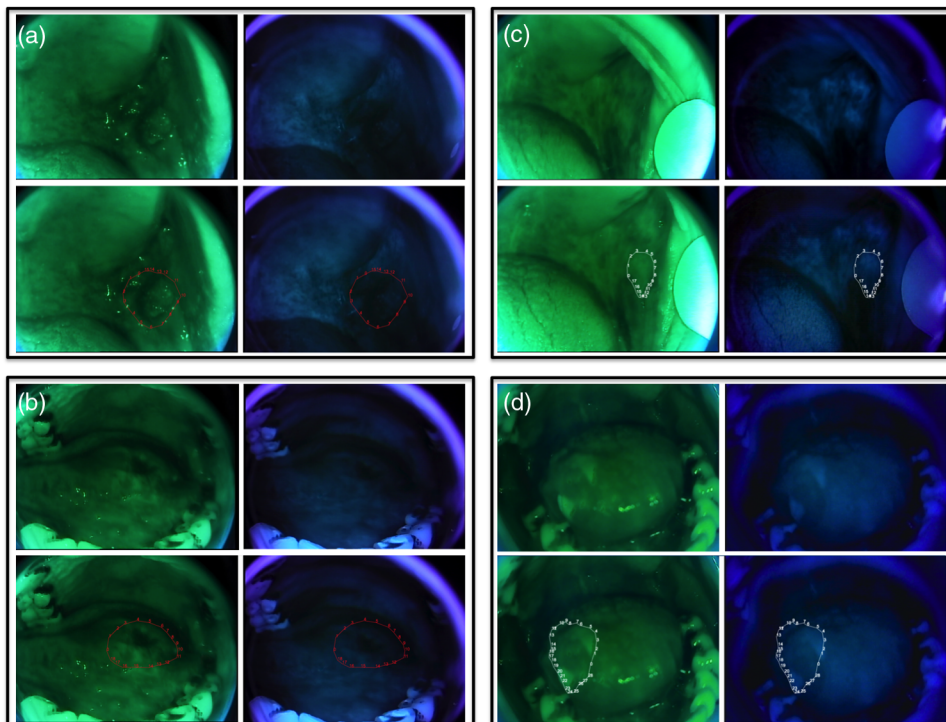

Fig. 3 The autofluorescence images in this study. In each image, upper left is 525 nm, upper right is 479 nm; lower is the lesion site of ROI. (a) Buccal mucosa cancer, (b) tongue cancer, (c) buccal mucosa squamous hyperplasia, and (d) tongue squamous hyperplasia.

$$I_r(x, y) = \frac{I_n(x, y)}{I_n(x, y) + I_f(x, y)}. \tag{1}$$

After applying Eq. (1) with $I_f(x, y)$ and $I_n(x, y)$, we can get a redox ratio image $I_r(x, y)$ and calculate the mean of ROI ω_r (Fig. 3).

We also calculated the heterogeneity index of the redox ratio using standard deviation. The heterogeneity of redox ratio H is defined as

$$H = \sqrt{\frac{\sum [I_r(x, y) - \omega_r]^2}{n}}, \tag{2}$$

where n is the number of pixels in ROI, and ω_r is the mean of the redox ratio.

2.2.5 Classification

Linear discriminant analysis (LDA) is often used in medical imaging to find a linear boundary that separates classes of objects. Quadratic discriminant analysis (QDA) is an extension of LDA; it separates classes of objects using a quadric surface and more powerful discriminates between them than does LDA. Therefore, we used the QDA algorithm described in Ref. 7.

In data analysis, we calculate the mean intensity and heterogeneity of the ROI in the NADH and FAD autofluorescence images and the redox ratio image and used the QDA algorithm for these data.

3 Results

The experimental group consisted of 49 biopsy-confirmed sets of oral cancer data and 34 sets of precancerous squamous hyperplasia data. The control group consisted of 77 sets of healthy (neither cancerous nor precancerous) data. All datasets were from May 18, 2015, to July 1, 2017. Each group was classified based on oral tissue from the buccal mucosa, tongue, lip, and palate (Table 1, data file 1).[23]

The QDA classifier was used to discriminate between the cancer and control groups. We defined the boundaries of the two groups, and, after they had been QDA classified, we calculated the sensitivity and specificity of the boundaries.

3.1 Autofluorescence Heterogeneity versus Intensity

The NADH (479 nm) QDA analysis of heterogeneity versus intensity showed a boundary with a specificity of 0.935 and a sensitivity of 0.735 for the control group and the cancer group, respectively [Fig. 5(a)]. The red area represents the control group, and the blue represents the cancer group.

The FAD (525 nm) QDA analysis of heterogeneity versus intensity showed a boundary a specificity of 0.935 and a sensitivity of 0.755 for the control group and the cancer group, respectively [Fig. 5(b)].

The cancerous and precancerous datasets were assigned to an abnormal group and compared with the control group. The NADH (479 nm) of heterogeneity and its intensity showed a boundary with a specificity of 0.870 and a sensitivity of 0.699 for the control group and the abnormal group [Fig. 5(c)], respectively. The red area represents the control group, and the blue represents the abnormal group.

Table 1 Dataset tissue site of patients (cancer stage base on AJCC seventh edition, 2010).

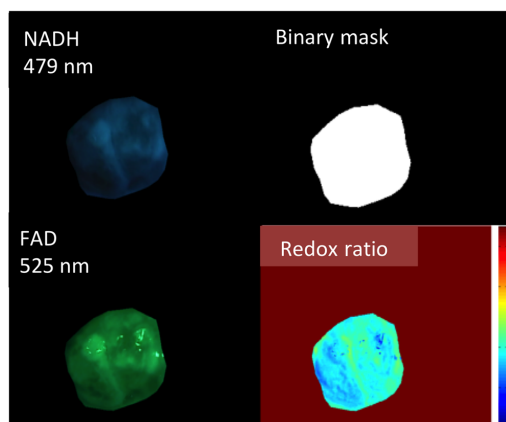|	Cancer $n = 49$	Precancer $n = 34$	Healthy $n = 77$
Site			
Buccal mucosa	30	19	38
Tongue	16	11	20
Lip	2	4	13
Palate	1	0	6
Age (years)			
Range/mean	35 to 91/59	47 to 85/61	19 to 90/43
Sex (M/F)	47/2	34/0	49/28
Diagnosis	Squamous cell carcinoma	Squamous hyperplasia	Healthy mucosa
Stage			
I	18		
II	9		
III	6		
IV	16		

Fig. 4 The binary mask and the images after applying the mask.

The QDA analysis of the heterogeneity of the FAD (525 nm) and its intensity showed a boundary with a specificity of 0.818 and a sensitivity of 0.663, respectively [Fig. 5(d)].

3.2 Autofluorescence Heterogeneity of Redox Ratio versus Intensity

We compared the autofluorescence heterogeneity of the redox ratio and its intensity among the cancer and abnormal group with the control group.

The QDA analysis of the heterogeneity of the redox ratio and NADH (479 nm) intensity showed a boundary with a specificity of 0.948 and a sensitivity of 0.898 for the control and cancer
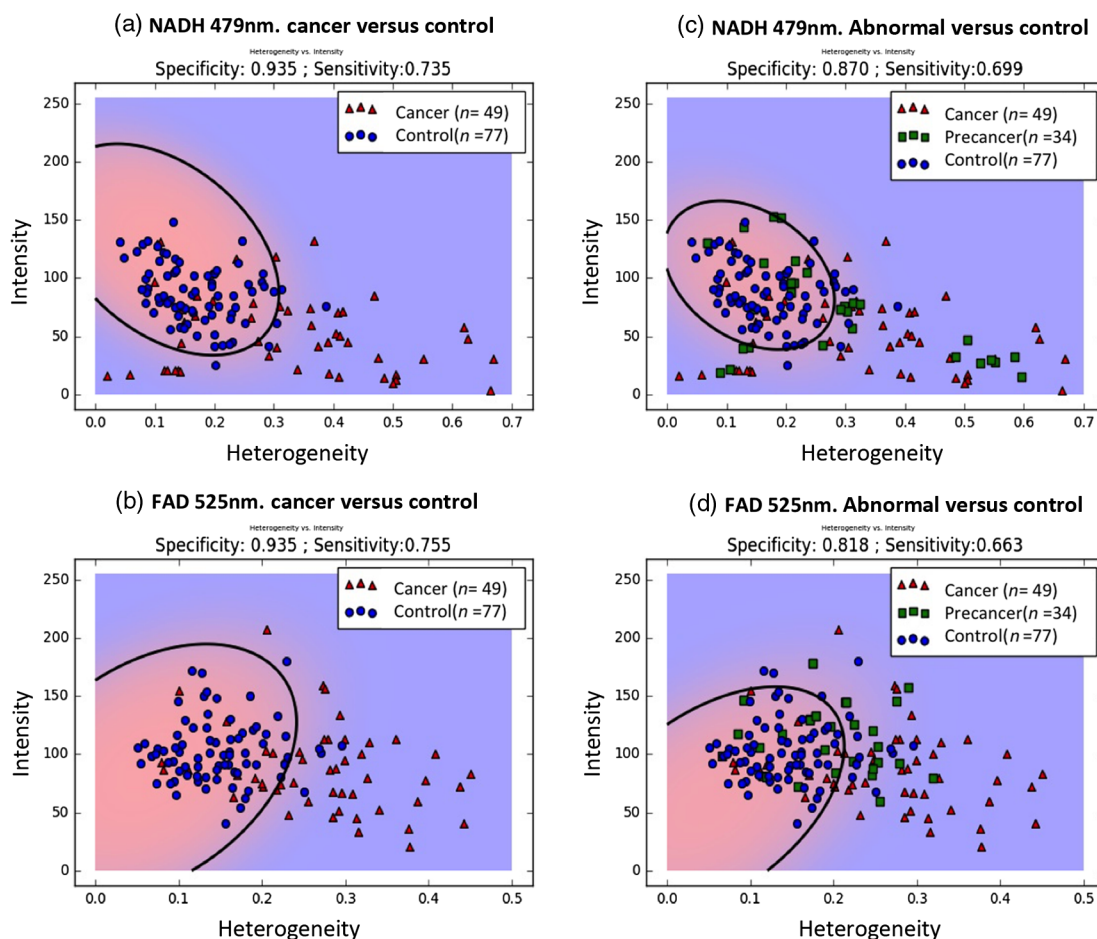
(a) **NADH 479nm. cancer versus control**

Heterogeneity vs. Intensity
Specificity: 0.935 ; Sensitivity:0.735

(c) **NADH 479nm. Abnormal versus control**

Heterogeneity vs. Intensity
Specificity: 0.870 ; Sensitivity:0.699

(b) **FAD 525nm. cancer versus control**

Heterogeneity vs. Intensity
Specificity: 0.935 ; Sensitivity:0.755

(d) **FAD 525nm. Abnormal versus control**

Heterogeneity vs. Intensity
Specificity: 0.818 ; Sensitivity:0.663

Fig. 5 (a) and (b) QDA classification of NADH (479 nm) and FAD (525 nm) autofluorescence intensity and heterogeneity based on the cancer and control groups. (c), (d) QDA classification of NADH (479 nm) and FAD (525 nm) autofluorescence intensity and heterogeneity based on the abnormal (cancer and precancer groups) and control groups.

groups, respectively [Fig. 6(a)]. The red area represents the control group, and the blue represents the cancer group.

The QDA analysis of the heterogeneity of the redox ratio and FAD (525 nm) intensity showed a boundary with a specificity of 0.948 and a sensitivity of 0.776 for the control and cancer groups, respectively [Fig. 6(b)].

The QDA analysis of the heterogeneity of the redox ratio and its NADH (479 nm) intensity showed a boundary with a specificity of 0.870 and a sensitivity of 0.771 for the control and abnormal groups, respectively [Fig. 6(c)]. The red area represents the control group, and the blue represent the abnormal group.

The QDA analysis of the heterogeneity of the redox ratio and its FAD (525 nm) intensity showed a boundary with specificity of 0.870 and sensitivity of 0.747, respectively [Fig. 6(d)].

There were five variants detected in this study: the NADH heterogeneities, NADH intensities, FAD heterogeneities, FAD intensities, and the redox ratio (NADH/NADH + FAD). All five variants were calculated for further QDA classification. The sensitivity of 0.974 and specificity of 0.898 of the boundaries between the oral cancer lesions and healthy oral mucosae were differentiated. The oral cancer and precancerous lesions were also differentiated from healthy oral mucosae: sensitivity = 0.919 and specificity = 0.755, respectively (Table 2).

To validate our findings, we randomly selected seven healthy and seven cancerous datasets of redox ratio versus NADH intensity results and ran the QDA classifier. The 14 validation group patients' data were then plotted (Appendix B). Total 56 healthy and 56 cancerous test set in eight runs of validation were performed with the specificity of 0.946 and sensitivity of 0.857 (Appendix B).

We also investigated the differentiation between the precancer and control groups (Appendix C). The QDA analysis of the heterogeneity of the redox ratio and its NADH (479 nm) intensity showed a boundary with a specificity of 0.948 and a sensitivity of 0.559.

4 Discussion

We designed a two-channel autofluorescence detection device to measure redox ratios of oral mucosae because no commercial device capable of doing that was available. It was (a) a handheld device with LEDs at 375 and 460 nm as an excitation light source for NADH and FAD, (b) a CCD camera covered with filters at 479 and 525 nm to generate an autofluorescence image, and (c) a minimotor to switch filters. This device was connected to a computer to instantly view the image. The redox ratio has always been difficult to verify because the NADH and FAD autofluorescence images must be taken at the same time
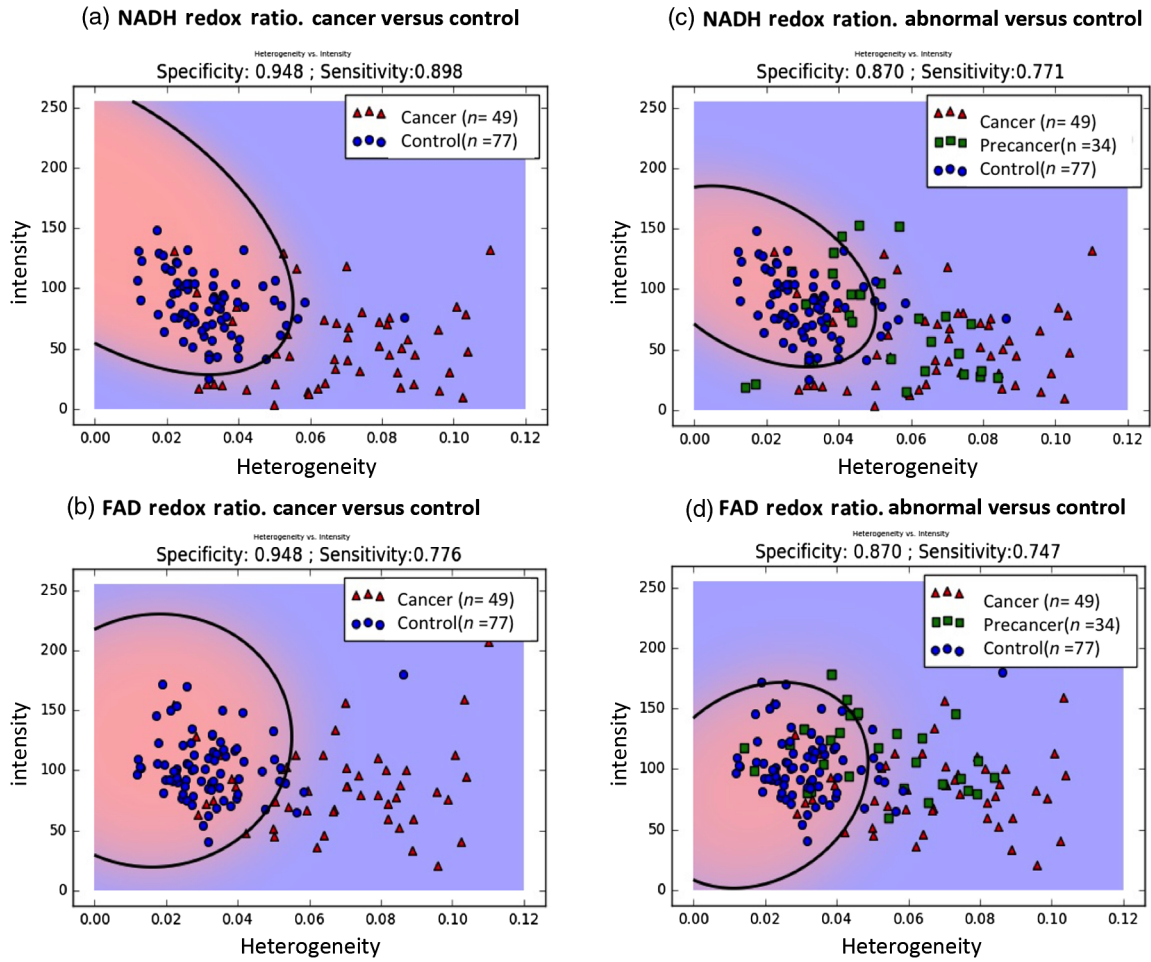
Fig. 6 (a) and (b) QDA classification of NADH (479 nm) and FAD (525 nm) autofluorescence intensity and heterogeneity index of the redox ratio based on the cancer and control groups. (c) and (d) QDA classification of NADH (479 nm) and FAD (525 nm) autofluorescence intensity and heterogeneity index of the redox ratio based on the abnormal (cancer and precancer groups) and control groups.

Table 2 The five variants of the NADH heterogeneities, NADH intensities, FAD heterogeneities, FAD intensities, and the heterogeneity of the redox ratio (NADH/NADH + FAD) were calculated for QDA classification of sensitivity and specificity.

Five dimensions QDA classifier

NADH intensity—NADH heterogeneity—FAD intensity—FAD heterogeneity—redox ratio		
	Sensitivity	Specificity
Oral cancer versus control	0.974	0.898
Abnormal versus control	0.919	0.755

and in the same place. Our device was developed with two excitation light sources, and it used different filters to record the autofluorescences at the same time and in the same place. We also selected the ICP algorithm[22] to correct the difference in location between the two images and developed algorithm for the measurement of pixel-wise redox ratio. The redox ratio implied that the cell was in the hypoxic state or that it

was in the active state and it was used to show the metabolic differences between healthy and tumorous tissue[17] when screening for oral cancer.

In routine clinical practice, oral mucosa lesions are detected primarily using direct visualization and palpation of soft tissue using instruments that facilitate visualization. The diagnosis is confirmed using a traditional biopsy in addition to some supplementary techniques. Although a biopsy is a minor procedure, high-risk patients are often reluctant to be screened for many reasons, including fear. Visual oral screening might reduce deaths from oral cancer worldwide, and reduce public health costs.[24,25] Other studies have used 100-W mercury arc lamp with narrow-band illumination filters at 420, 430, 530, and 600 nm[26,27] and blue (405 nm) and white LEDs without filter[28] for pilot studies of oral neoplasia. We used specific excitation light source and filters to detect autofluorescence in 160 patients. All the data acquired in this study were high-specificity and high-sensitivity for oral neoplasia. Several commercial instruments have also been developed for routine examination: the ViziLite® (Zila Pharmaceuticals, Phoenix, Arizona), VELscope® (Visually Enhanced Lesion Scope; LED Dental Inc., White Rock, B.C., Canada), and OralCDx® (CDx® Diagnostics, Suffern, New York). These devices all consist of

a light source, where the emitted fluorescence is directly visualized.[29] There were two light sources of our device with two filters; therefore, early biochemical changes can be detected before gross alteration, which permits early detection of pathological lesions. Most metabolic activity occurs inside mitochondria. Our device detected the FAD and NADH intensity to distinguish between different metabolic stages autofluorescence intensities changes.[30] The redox ratio has been used to show the metabolic differences between healthy tissue and tumors between indolent and aggressive tumors.[16,17,31,32] Our device records the autofluorescences at the same time and in the same place. We also developed algorithm to measure the pixel-wise redox ratio.

Our study has some limitations. First, although our device has the advantage of being a two-channel system, it is not as small as a fiber-optic system.[33] Second, the oropharyngeal area of the oral cavity could not be excited by LEDs, or by an out-of-focus CCD camera because of its fixed-focus lens. Because of its size, our device could simultaneously capture only two autofluorescence images. The white-light images had to be captured by another device. To use our device in the nasopharyngeal, oropharyngeal, and hypopharyngeal areas, it would have to be a fiber-optic system. Third, the white-light reference image was not taken at the same time because there was no space to put a white-light LED and extra filter in our current device. Currently, physicians normally use a white light to examine lesion with the naked eye. Not having a white-light image might cause a user obstacle when reading the autofluorescence images. Fourth, the moisture that accumulates when the patient breathes often covers the LEDs, lenses, and filters with water vapor and causes fuzzy photos. Unless the device is ventilated, targeted patients will have to hold their breath while the autofluorescence images are being captured. Fifth, we had few samples datasets for 49 oral cancers, 34 precancers, and 77 healthy oral mucosae. Many more datasets are required to validate our findings.

The heterogeneity index of the redox ratio is the heterogeneous value of the redox ratio. The five variants of the NADH heterogeneities, NADH intensities, FAD heterogeneities, FAD intensities, and the heterogeneity of redox ratio (NADH/NADH + FAD) were most powerful for discriminating cancerous, precancerous, and healthy tissue using the QDA classifier. An animal study[31] also showed redox ratio changes in rat brain tumors but not in the surrounding healthy brain tissue. Other animal studies[17] have also reported that indolent tumors have more redox ratio change than do aggressive tumors. The lower specificity and sensitivity for identifying abnormal tissue might be because of the wide range of oral lesions, which might have features like those of healthy oral mucosa or cancerous lesions. Aggressive surgical excision or laser therapy combined with a close follow-up of these precancerous lesions with autofluorescence features like those of oral cancer might be advisable. Additional long-term studies should be done to clinically validate these autofluorescence features in precancerous lesions. Likewise, precancerous lesions with autofluorescence features like those of healthy oral mucosa might indicate benign behavior; thus, additional follow-ups are warranted.

Our algorithm enabled us to discriminate between oral cancerous, precancerous, and healthy oral mucosae. Because of its high sensitivity, automatic identification of lesion boundaries could be used to determine the surgical margins required during lesion ablation. In an early oral cancerous lesion, it might also be difficult to determine the necessity of a tissue biopsy because of nonsignificant clinical features. Our two-channel system can also help with this determination.

5 Conclusion

We designed a two-channel autofluorescence detection device to measure intensity, heterogeneity of NADH and FAD, and redox ratios of oral mucosae, and a quantitative analysis technique were developed to screen and diagnose precancerous and cancerous lesions of the oral cavity. Our device and analytical method yielded high-sensitivity and high-specificity results when combined with a QDA classifier.

Our autofluorescence imaging technique can be used for oral cancer screening and, perhaps, other types of cancer if we can solve some device problems: size, water vapor, and white-light reference not combined in the same device. Additional long-term studies are required to confirm the value of our clinical method.

Table 3 Total 56 normal and 56 cancer test set in eight runs of validation with specificity of 0.946 and sensitivity of 0.857, respectively.

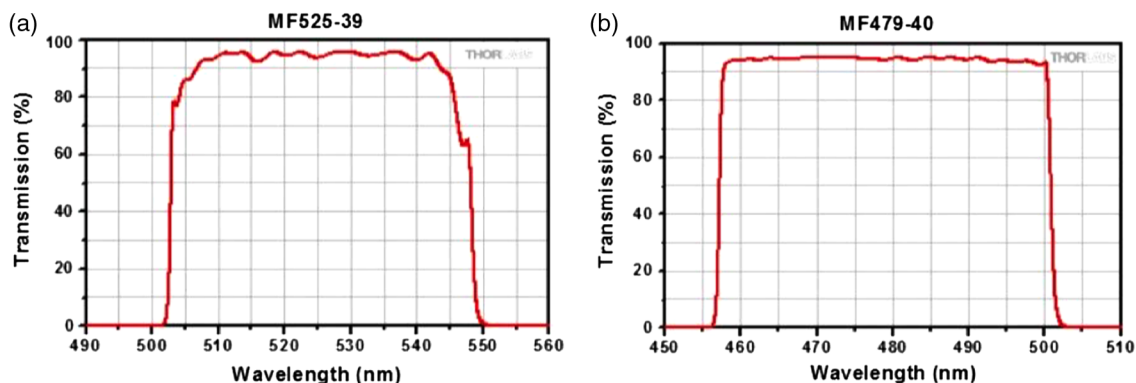|	Classified as normal	Classified as cancer
Normal	53	3
Cancer	8	48

Fig. 7 Filter specification of the device (a) 525-nm filter and (b) 479-nm filter.
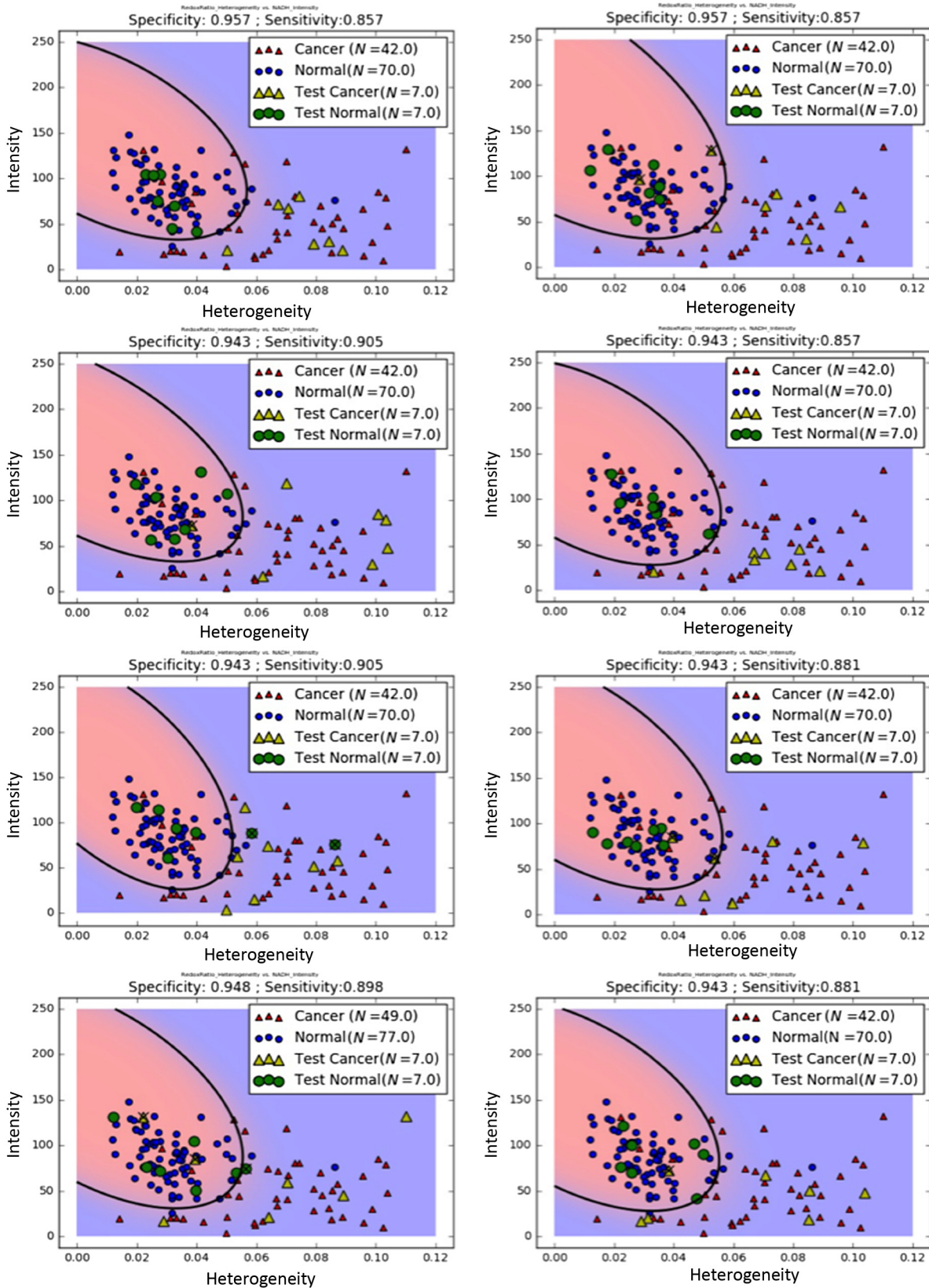
Fig. 8 Randomly selected seven normal and seven cancer out of dataset of the redox ratio versus NADH intensity and ran the QDA classifier. The 14 patients' data were then plotted in as testing.

Appendix A

The parameters and specifications of the device.

LED specification.
UV LED: NSSU123T—peak wavelength: 375 nm, radiant flux: 17.6 mW, spectrum half width: 9 nm.
Blue LED: KA-3529AQB25Z4S—peak wavelength: 460 nm, spectrum half width: 20 nm.

Exposure times: 0.5 s

Filter specification of the device. Figure 7(a): 525-nm filter. Figure 7(b): 479-nm filter.

Appendix B

To validate our findings, we randomly selected seven healthy and seven cancerous datasets of redox ratio versus NADH intensity results and ran the QDA classifier. The 14 validation group patients' data were then plotted (Table 3). Totally, 56 healthy and 56 cancerous test set in eight runs of validation were performed with the specificity of 0.946 and sensitivity of 0.857 (Fig. 8).

Appendix C

We compared the autofluorescence heterogeneity of the redox ratio versus intensity. The analysis was also according to precancer versus control group.

The QDA analysis of the heterogeneity and intensity of NADH (479 nm) showed a boundary with a specificity of 0.974 and a sensitivity of 0.382, respectively, for the control and the precancer groups [Fig. 9(a)]. The red area represents the control and the blue represents the precancer groups.

The QDA analysis of the heterogeneity and intensity of FAD (525 nm) showed a boundary with a specificity of 0.896 and a sensitivity of 0.412, respectively, for the control and precancer groups [Fig. 9(b)].

The QDA analysis of the heterogeneity of the redox ratio versus NADH (479 nm) intensity showed a boundary with a specificity of 0.948 and a sensitivity of 0.559, respectively, for the control and the precancer groups [Fig. 9(c)]. The red area represents the control group, and the blue represent the precancer group.

The QDA analysis of the heterogeneity of the redox ratio versus FAD (525 nm) intensity showed a boundary with specificity of 0.909 and sensitivity of 0.618 [Fig. 9(d)].
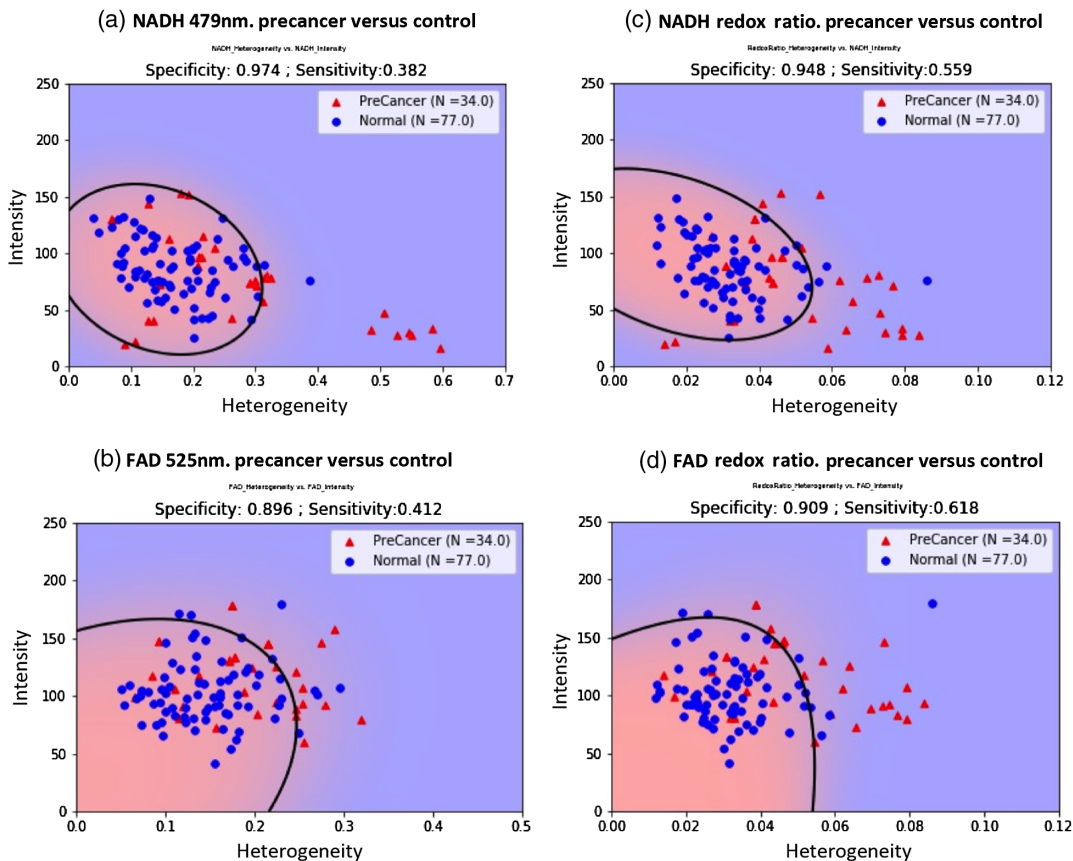

Fig. 9 (a) and (b) QDA classification of NADH (479 nm) and FAD (525 nm) autofluorescence intensity and heterogeneity index of the redox ratio based on the precancer and control groups. (c) and (d) QDA classification of NADH (479 nm) and FAD (525 nm) autofluorescence intensity and heterogeneity index of the redox ratio based on the precancer group and control groups, respectively.

References

1. C.-C. Su et al., "Distinctive features of oral cancer in Changhua County: high incidence, buccal mucosa preponderance, and a close relation to betel quid chewing habit," *J. Formos. Med. Assoc.* **106**(3), 225–233 (2007).
2. A. C. Chi, T. A. Day, and B. W. Neville, "Oral cavity and oropharyngeal squamous cell carcinoma—an update," *CA Cancer J. Clin.* **65**(5), 401–421 (2015).
3. A. K. Chaturvedi et al., "Worldwide trends in incidence rates for oral cavity and oropharyngeal cancers," *J. Clin. Oncol.* **31**(36), 4550–4559 (2013).
4. S. Marur and A. A. Forastiere, "Head and neck squamous cell carcinoma: update on epidemiology, diagnosis, and treatment," *Mayo Clin. Proc.* **91**(3), 386–396 (2016).
5. T. Poate et al., "An audit of the efficacy of the oral brush biopsy technique in a specialist oral medicine unit," *Oral Oncol.* **40**(8), 829–834 (2004).
6. D. Roblyer et al., "Objective detection and delineation of oral neoplasia using autofluorescence imaging," *Cancer Prev. Res.* **2**(5), 423–431 (2009).
7. T. T. Huang et al., "Novel quantitative analysis of autofluorescence images for oral cancer screening," *Oral Oncol.* **68**, 20–26 (2017).
8. J. Epstein et al., "Analysis of oral lesion biopsies identified and evaluated by visual examination, chemiluminescence and toluidine blue," *Oral Oncol.* **44**(6), 538–544 (2008).
9. S. Barrett, "ViziLite screening: does it make sense?" https://www.dentalwatch.org/questionable/vizilite/overview.html (23 June 2018).
10. Y. Sun et al., "Fluorescence lifetime imaging microscopy: in vivo application to diagnosis of oral carcinoma," *Opt. Lett.* **34**(13), 2081–2083 (2009).
11. D. De Veld et al., "The status of in vivo autofluorescence spectroscopy and imaging for oral oncology," *Oral Oncol.* **41**(2), 117–131 (2005).
12. C. S. Farah et al., "Efficacy of tissue autofluorescence imaging (VELScope) in the visualization of oral mucosal lesions," *Head Neck* **34**(6), 856–862 (2012).
13. A. T. Shah et al., "In vivo autofluorescence imaging of tumor heterogeneity in response to treatment," *Neoplasia* **17**(12), 862–870 (2015).
14. N. Kollias, G. Zonios, and G. N. Stamatas, "Fluorescence spectroscopy of skin," *Vib. Spectrosc.* **28**(1), 17–23 (2002).
15. M. G. Vander Heiden, L. C. Cantley, and C. B. Thompson, "Understanding the Warburg effect: the metabolic requirements of cell proliferation," *Science* **324**(5930), 1029–1033 (2009).
16. J. H. Ostrander et al., "Optical redox ratio differentiates breast cancer cell lines based on estrogen receptor status," *Cancer Res.* **70**(11), 4759–4766 (2010).
17. H. N. Xu et al., "Quantitative mitochondrial redox imaging of breast cancer metastatic potential," *J. Biomed. Opt.* **15**(3), 036010 (2010).
18. R. Drezek et al., "Understanding the contributions of NADH and collagen to cervical tissue fluorescence spectra: modeling, measurements, and implications," *J. Biomed. Opt.* **6**(4), 385–396 (2001).
19. L. Z. Li et al., "Quantitative magnetic resonance and optical imaging biomarkers of melanoma metastatic potential," *Proc. Natl. Acad. Sci. U. S. A.* **106**(16), 6608–6613 (2009).
20. G. A. Wagnieres, W. M. Star, and B. C. Wilson, "In vivo fluorescence spectroscopy and imaging for oncological applications," *Photochem. Photobiol.* **68**(5), 603–632 (1998).
21. http://www.sgs.com/en/our-company/about-sgs/sgs-in-brief
22. G. Vasilakos et al., "Assessment of different techniques for 3D superimposition of serial digital maxillary dental casts on palatal structures," *Sci. Rep.* **7**(1), 5838 (2017).
23. T. Huang, "Two-channel autofluorescence analysis for oral cancer," *Figshare*, 2018, https://figshare.com/s/ba89264862a0f76ab0a5 (19 January 2018).
24. P. Brocklehurst et al., "Screening programmes for the early detection and prevention of oral cancer," *Cochrane Database Syst. Rev.* **10**(11), CD004150 (2013).
25. M. D. Mignogna and S. Fedele, "Oral cancer screening: 5 minutes to save a life," *Lancet* **365**(9475), 1905–1906 (2005).
26. R. Nagi et al., "Efficacy of light based detection systems for early detection of oral cancer and oral potentially malignant disorders: systematic review," *Med. Oral. Patol. Oral Cir. Bucal* **21**(4), e447–e455 (2016).
27. D. Roblyer et al., "Multispectral optical imaging device for in vivo detection of oral neoplasia," *J. Biomed. Opt.* **13**(2), 024019 (2008).
28. N. Bedard et al., "Multimodal snapshot spectral imaging for oral cancer diagnostics: a pilot study," *Biomed. Opt. Express* **4**(6), 938–949 (2013).
29. C. F. Poh et al., "Fluorescence visualization detection of field alterations in tumor margins of oral cancer patients," *Clin. Cancer Res.* **12**(22), 6716–6722 (2006).
30. B. Chance et al., "Oxidation-reduction ratio studies of mitochondria in freeze-trapped samples. NADH and flavoprotein fluorescence signals," *J. Biol. Chem.* **254**(11), 4764–4771 (1979).
31. Q. Liu et al., "Compact point-detection fluorescence spectroscopy system for quantifying intrinsic fluorescence redox ratio in brain cancer diagnostics," *J. Biomed. Opt.* **16**(3), 037004 (2011).
32. K. Cai et al., "Characterizing prostate tumor mouse xenografts with CEST and MT-MRI and redox scanning," *Adv. Exp. Med. Biol.* 39–45 (2013).
33. G. A. Grillone et al., "The color of cancer: margin guidance for oral cancer resection using elastic scattering spectroscopy," *Laryngoscope* **127**(Suppl. 4), S1–S9 (2017).

Tze-Ta Huang is an assistant professor and attending physician in the Division of Oral and Maxillofacial Surgery, Department of Stomatology, Institute of Oral Medicine, National Cheng Kung University Medical College and Hospital, Tainan, Taiwan. He received his DDS degree from the School of Dentistry, National Yang-Ming University, Taipei, Taiwan, in 1996, and his MSc and PhD degrees from the Institute of Molecular Biology, National Chung Cheng University, Minxiong Township, Chiayi County, Taiwan, 2005 and 2013, respectively. He has more than 10 published papers. His current research interests include oral carcinogenesis and optical imaging device.

Pau-Choo Chung is a professor in the Department of Electrical Engineering, National Cheng Kung University, Tainan, Taiwan.

Jehn-Shyun Huang is an associate professor and attending physician in the Division of Oral and Maxillofacial Surgery, Department of Stomatology, Institute of Oral Medicine, Medical College and Hospital, National Cheng Kung University, Tainan, Taiwan. He is the senior faculty with research experience of more than 25 years.

Biographies for the other authors are not available.